Optica Applicata, Vol. XLV, No. 3, 2015
DOI: 10.5277/oa150312

Theoretical investigation of slab waveguide sensor using anisotropic metamaterial

SOFYAN A. TAYA

Physics Department, Islamic University of Gaza, P.O.Box 108, Gaza, Palestinian Authority;
e-mail: staya@iugaza.edu.ps

A three-layer slab waveguide with air as a substrate, lossless dielectric as a guiding film, and anisotropic double negative material as a cladding is explored as an optical sensor for refractometry applications. The double negative material is assumed to have a negative electric permittivity and magnetic permeability only along the wave propagation direction. The sensitivity of a guided mode to the variation in the refractive index of air substrate is derived and studied for the first few guided modes. It is found that the sensitivity can be enhanced with decreasing the guided light frequency as well as the film thickness. The sensitivity can reach 100% for some waveguide configurations.

Keywords: anisotropic waveguides, optical sensing, double negative materials.

1. Introduction

In the last two decades, slab waveguide sensors have played a remarkable role in chemical and biological sensing applications [1–5]. Much progress has been observed in the field of slab waveguide sensors over the last two decades due to their advantageous features with respect to electric sensors such as rapid response, direct detection, and immunity to electromagnetic interference. Moreover, they have small size and weight and can be used in aggressive and ionizing environments. The latest trends in optical waveguide sensors include compatibility with mass production processes and multiple analyte detection. Another significant feature of slab waveguide sensors is that they are easy to interface with optical data communication systems. Optical sensors are classified according to sensing architecture and mechanism. There are various architecture slab waveguide configurations such as mode waveguides, surface plasmon resonance, metal clad waveguides, interferometers, anti-resonant reflecting optical waveguides, Bragg gratings, integrated optical microcavities, and silicon slot waveguides. On the other hand, there are a set of sensing mechanisms such as modal index of refraction change in the guiding structures, fluorescence, surface plasmon resonance, Raman scattering, and absorption change. It is worth comparing between planar waveguide sensor and some other sensors. The principle of operation of mode waveguide sensor is based on the evanescent field penetrating the analyte layer from the guiding layer and senses the changes in the index of refraction of the analyte. The sens-

ing principle of metal-clad waveguide and surface plasmon resonance sensors is to measure the reflectance as a function of the angle of incidence. The use of metal-clad waveguide and surface plasmon resonance structures as optical sensors is based on measuring the angular shift in the reflectance dip/peak when the index of refraction of the analyte changes. A cavity ring-down [5] setup involves an optical cavity made from two or three mirrors. Light is coupled into the cavity through one of the mirrors and light leaking out of the cavity is detected. When a cavity resonance is excited, power builds up in the cavity and then decays exponentially as the light source is switched off. The decay time is a direct measure of the optical loss in the cavity. In cavity ring-down spectrometers the optical loss is changed by filling the cavity, at least in part, with an absorber, which can then be quantified. Most cavity ring-down spectrometers are designed for very sensitive gas absorption measurements and have volumes of tens to hundreds of milliliters.

Slab waveguide sensors can be used to measure almost any external parameter such as chemical and biological parameters with high accuracy and speed. Biosensors are used to measure the presence of biological molecules and micro-organisms by converting biochemical interactions at the probe surface into a measurable signal. Biosensors have wide applications in drug industry, diagnostics, and medical tests. Intensive research has been carried out to develop biosensors for fast and sensitive detection and has resulted in various efficient techniques [6–21].

Currently double negative materials (DNMs) have received a lot of interest by the scientific community [22–47] due to their potential applications such as absorbers, filters, couplers, antennas, and superprisms. These media are known as "metamaterials" and are quite different from the conventional ones. One of the most important feature of these materials is the negative index of refraction. Although such a phenomenon was initially met with some doubt [24], numerical simulation [26] and experimental evidence [27] have proved the existence of negative refraction. The mechanism of negative refractive index can be divided into local resonance and non-local Bragg scattering. There is no limit imposed on the sizes of the lattice constants in the local resonance mechanism in which the period of the structure could be much smaller than the working wavelength. DNMs belonging to this mechanism are approximated to be isotropic homogeneous media [28]. VESELAGO first pointed out DNMs with simultaneously negative electric permittivity and magnetic permeability in 1968 [23]. Few decades later, several theoretical and experimental groups have investigated DNMs due to their potential applications in a set of interesting applications.

The main aim of the current work is to propose a slab waveguide sensor of high sensitivity utilizing DNM taking into account the real properties of DNMs such as loss, dispersion and anisotropy.

In recent studies, slab waveguide sensors utilizing DNMs were proposed and analyzed. Reverse index slab waveguide sensor with DNM guiding layer was investigated [48]. The proposed four-layer structure was found to have larger adlayer sensitivity over conventional slab waveguide sensors having a dielectric material in the guiding layer. Sensitivities of three and four layer slab waveguide structures having

DNM films were derived and compared [49]. It was found that the DNM enhances the cover layer as well as the adlayer sensitivities. The novelty of the current work in comparison with the studies presented in [48, 49] is taking into account the dispersion and anisotropy properties of the DNM which were ignored in previous studies.

In this paper, a three-layer slab waveguide structure is treated as an optical sensor for refractometry applications. The substrate contains the material to be detected (analyte). The guiding film and cladding are assumed to be a lossless dielectric and an anisotropic DNM, respectively. The sensitivity of the proposed sensor is investigated with the frequency of the guided light for different transverse electric (TE) modes. The effect of the anisotropy of the cladding layer on the sensitivity is also explored.

2. Mathematical analysis

Figure 1 shows a schematic of slab waveguide sensor configuration in which the analyte medium is located in the substrate. The waveguide comprises three layers: substrate with parameters ε_1 and μ_1, guiding film of thickness h and parameters ε_2 and μ_2, and anisotropic DNM in which $[\varepsilon_3]$ and $[\mu_3]$ are given as tensors. Each tensor contains only three non-zero elements. The DNM cladding is assumed to exhibit negative parameters in the longitudinal direction only, *i.e.*, $\varepsilon_{3z} < 0$, $\mu_{3z} < 0$, $\varepsilon_{3x} > 0$, $\varepsilon_{3y} > 0$, $\mu_{3x} > 0$, and $\mu_{3y} > 0$. The longitudinal components of $[\varepsilon_3]$ and $[\mu_3]$ are given by the empirical relationships

$$\varepsilon_{3z} = 1 - \frac{\omega_p^2}{\omega^2 + i\Gamma_e \omega} \tag{1}$$

$$\mu_{3z} = 1 - \frac{F\omega^2}{\omega^2 - \omega_o^2 + i\Gamma_m \omega} \tag{2}$$

where ω_p is the plasma frequency, ω_o is the resonance frequency, Γ_e and Γ_m are the electric and magnetic loss factors, ω is the angular frequency, and F is the fractional area of the unit cell occupied by the split ring.

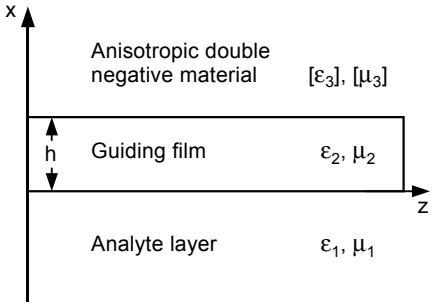

Fig. 1. Schematic geometry of a three-layer slab waveguide structure including an anisotropic DNM as a cladding layer.

The wave equation in the anisotropic DNM cladding for TE_m modes is given by

$$\frac{\partial^2 E_y(x)}{\partial x^2} - \left(\frac{\beta^2 \mu_{3z}}{\mu_{3x}} - \omega^2 \varepsilon_0 \mu_0 \varepsilon_{3y} \mu_{3z} \right) E_y(x) = 0 \tag{3}$$

whereas in the guiding film and substrate it is given by

$$\frac{\partial^2 E_y(x)}{\partial x^2} - (\beta^2 - k_0^2 \varepsilon_i \mu_i) E_y(x) = 0, \quad i = 1, 2 \tag{4}$$

where k_0, ε_0, and μ_0 are the free space wave number, permittivity, and permeability, respectively; β is the longitudinal propagation constant. The solutions of the wave equations in the three media of the waveguide structure are given by

$$E_y(x) = E_1 \exp(q_1 x), \quad x < 0 \tag{5}$$

$$E_y(x) = E_2 \cos(q_2 x - d), \quad 0 < x < h \tag{6}$$

$$E_y(x) = E_3 \exp[-q_3 (x - h)], \quad x > h \tag{7}$$

where

$$q_1 = \sqrt{\beta^2 - k_0^2 \varepsilon_1 \mu_1} \tag{8}$$

$$q_2 = \sqrt{k_0^2 \varepsilon_2 \mu_2 - \beta^2} \tag{9}$$

$$q_3 = \sqrt{\frac{\mu_{3z}}{\mu_{3x}} (\beta^2 - k_0^2 \varepsilon_{3y} \mu_{3x})} \tag{10}$$

Two non-zero components of the magnetic field exist: $H_x(x)$ and $H_z(x)$. They can be calculated in the anisotropic DNM using $H_x = -\beta/(\omega \mu_0 \mu_{3x}) E_y$ and $H_z = i/(\omega \mu_0 \mu_{3z}) \times \times \partial E_y/\partial x$ whereas they can be calculated in the guiding film and substrate using $H_x = = -\beta/(\omega \mu_0 \mu_i) E_y$ and $H_z = i/(\omega \mu_0 \mu_i) \partial E_y/\partial x$. As tangential components, both $E_y(x)$ and $H_z(x)$ are continuous. Applying the continuity of these components at $x = 0$ and $x = h$, the characteristic equation is obtained which is given by

$$q_2 h - \tan^{-1}(\varphi_3) \tan^{-1}(\varphi_1) - m\pi = 0 \tag{11}$$

where $\varphi_3 = \dfrac{\mu_2 q_3}{\mu_{3z} q_2}$, $\varphi_1 = \dfrac{\mu_2 q_1}{\mu_1 q_2}$, and $m = 0, 1, 2, \ldots$ is the mode number.

Equation (11) has to be solved numerically for the longitudinal propagation constant β which can be written as $\beta = k_0 N$ with N being the modal index of refraction of the guided mode.

When the index of refraction of the analyte layer undergoes any change due to any contamination, the modal index changes. This change in N is the sensing probe used to detect any changes in the index of the analyte. The sensitivity of the slab waveguide is defined as the rate of change of the modal index under an index change of the analyte, *i.e.*, $S = \partial N/\partial n_1$, where $n_1 = (\varepsilon_1\mu_1)^{1/2}$ is the index of refraction of the analyte layer. Differentiating Eq. (11) with respect to N, we get

$$S = \frac{\mu_1\mu_2 q_2^2 k_0^2 n_1}{\tau_2\left(\frac{\tau_1}{\tau_2} + \frac{\tau_3}{\tau_4} + \frac{k_0^2 Nh}{q_2}\right)} \tag{12}$$

where

$$\tau_1 = \mu_1\mu_2 k_0^2 N(q_1^2 + q_2^2) \tag{13}$$

$$\tau_2 = q_1 q_2(\mu_1^2 q_2^2 + \mu_2^2 q_1^2) \tag{14}$$

$$\tau_3 = \mu_2\mu_{3z} k_0^2 N(\mu_{3z} q_2^2 + \mu_{3x} q_3^2) \tag{15}$$

$$\tau_4 = \mu_{3x} q_2 q_3(\mu_{3z}^2 q_2^2 + \mu_2^2 q_3^2) \tag{16}$$

3. Numerical results

In the following simulation, the guiding film of the waveguide is assumed to be silicon nitride (Si_3N_4) with parameters $\varepsilon_2 = 4.04$, $\mu_2 = 1$, and $n_f = (\varepsilon_2\mu_2)^{1/2} = 2.01$ and the analyte layer is air with $\varepsilon_1 = \mu_1 = 1$ and $n_s = (\varepsilon_1\mu_1)^{1/2} = 1.0$. Uniaxial anisotropic DNM is considered to exist in the cladding region in which the longitudinal permittivity and permeability are negative and dispersive as given by Eqs. (1) and (2), respectively, whereas the transverse components are positive and are given by $\varepsilon_{3x} = \varepsilon_{3y} = 2.25$ and $\mu_{3x} = \mu_{3y} = 1$ ($n_{cx} = n_{cy} = (\varepsilon_{3x}\mu_{3x})^{1/2} = 1.50$). The DNM cladding is assumed to be lossy material and have the parameters $F = 0.56$, $\omega_0 = 4$ GHz, $\omega_p = 10$ GHz, and $\Gamma_e = \Gamma_m = 0.012\omega_p$. The characteristic equation was solved numerically in the frequency range 4.0 GHz < ω < 6.0 GHz and the sensitivity of the waveguide structure to any change in the index of the analyte layer was calculated using Eq. (12). The longitudinal refractive index of DNM can be calculated using Eqs. (1) and (2). For example, at $\omega = 6$ GHz, $n_{cz} = (\varepsilon_{3z}\mu_{3z})^{1/2} = [(-1.78 + 0.06i)(-0.007 + 0.04i)]^{1/2}$. The sensitivity of the proposed sensor *versus* the angular frequency of the guided light is shown in Fig. 2 for the fundamental mode. The fundamental mode (TE_0) is found to exist in the frequency range 4.0 GHz < ω < 4.4 GHz for guiding film thickness h range from 0.1 to 0.5 mm. The numerical simulation showed that the existence of a guided mode is crucially dependent on the thickness of the guiding film and the operating frequency range. As the figure reveals, the sensitivity decreases with increasing the frequency for a fixed

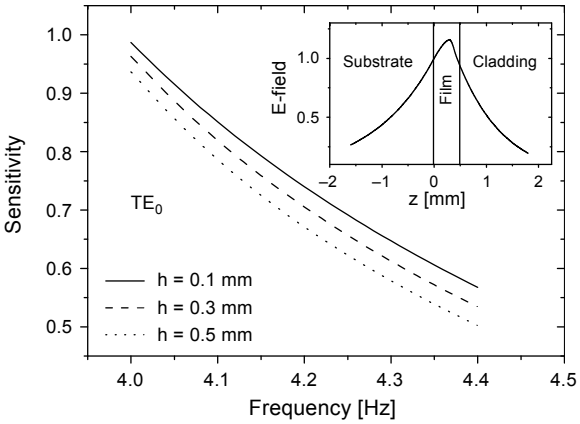

Fig. 2. Sensitivity *versus* angular frequency for the fundamental mode for different guiding film thicknesses for $\varepsilon_1 = 1$, $\mu_1 = 1$, $\varepsilon_2 = 4.04$, $\mu_2 = 1$, $\varepsilon_{3x} = \varepsilon_{3y} = 2.25$, and $\mu_{3x} = \mu_{3y} = 1$, $F = 0.56$, $\omega_0 = 4.0$ GHz, $\omega_p = 10.0$ GHz, and $\Gamma_e = \Gamma_m = 0.012\omega_p$. The inset shows the field profile for TE_0 mode for $h = 0.5$ mm.

guiding film thickness. This behavior can be attributed to the reduction of the penetration depth of the evanescent field into the analyte layer as the frequency of the guided light increases. As the frequency increases, the wavelength decreases and penetration depth of the wave in the surrounding media also decreases since it is comparable to the wavelength. Moreover, as the thickness of the guiding film increases for the same ω, the sensitivity decreases since increasing the thickness of the film enhances the confinement of the wave in the guiding film and reduces the evanescent field in the analyte layer. The sensitivity ranged between $0.99 \le S \le 0.57$ for $h = 0.1$ mm, $0.96 \le S \le 0.53$ for $h = 0.3$ mm, $0.94 \le S \le 0.50$ and for $h = 0.5$ mm.

To demonstrate the possibility of microbe detections, the electric field intensity profile across the structure layers was calculated and plotted in the inset of Fig. 2 for TE_0 mode. As can be seen from the inset, the field configuration is asymmetric, the evanescent field in the substrate region is larger than that in the cover region. The penetration depth of the evanescent field in a medium is defined as the distance from the interface at which the power of the electric field decreases to $1/e$ of its initial value [48]. From the inset of Fig. 2, the penetration depth of the evanescent field in the substrate region is 1.2 mm which is very high for the detection of micrometer-scale biological objects such as cells and bacteria.

The first guided mode was found to exist in the operating frequency band 4.2 GHz < ω < 5.7 GHz for h range from 2.0 to 2.2 cm as can be seen from Fig. 3. On the other hand, Fig. 4 shows that the second guided mode exists in the frequency range 4.2 GHz < ω < 5.7 GHz for h range from 4.0 to 4.2 cm. Figures 3 and 4 show that the sensitivities of the first and second guided modes have the same features as those of the sensitivity of the fundamental mode. It decays with increasing the guided wave fre-

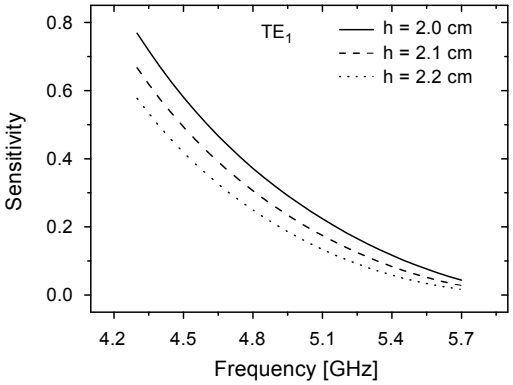

Fig. 3. Sensitivity *versus* angular frequency for the first guided mode for different guiding film thicknesses. The waveguide parameters are the same as in Fig. 2.

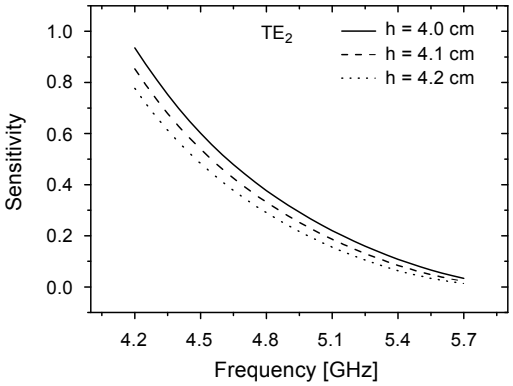

Fig. 4. Sensitivity *versus* angular frequency for the second guided mode for different guiding film thicknesses. The waveguide parameters are the same as in Fig. 2.

quency for a fixed film thickness and also decreases when the thickness of the film increases for the same ω.

Figure 5 shows the sensitivity *versus* the guiding film thickness for the first guided mode for $\omega = 4.5$ GHz. The thickness of the guiding film was varied from 1.87 to 2.4 cm in steps of 0.01 cm. As the figure shows, the sensitivity of the proposed waveguide structure is 100% when $h = 1.87$ cm and it decreases to 50% for $h = 2.4$ cm. This can be explained from the inset in the figure which shows the modal index of refraction *versus* the thickness of the guiding film. It shows that the modal index is equal to that of the analyte layer when $h = 1.87$ cm. This means that this thickness represents the cut-off thickness at which the entire wave propagates in the analyte layer and the modal index is equal to that of the substrate. If the analyte is located in the cladding region, the sensitivity corresponding to cut-off thickness is zero since the wave does

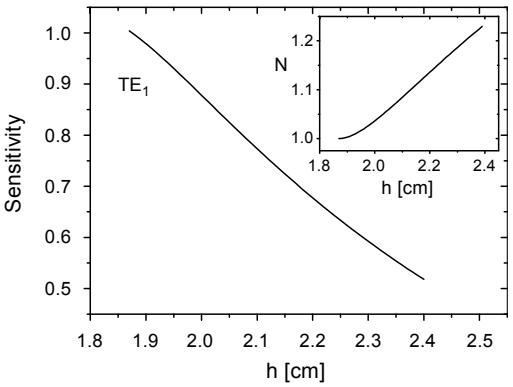

Fig. 5. Sensitivity *versus* guiding film thickness for $\omega = 4.5$ GHz at which $n_{cz} = [(-3.93 + 0.13i) \times (-1.63 + 0.33i)]^{1/2}$. The inset shows the modal index with the film thickness. The waveguide parameters are the same as in Fig. 2.

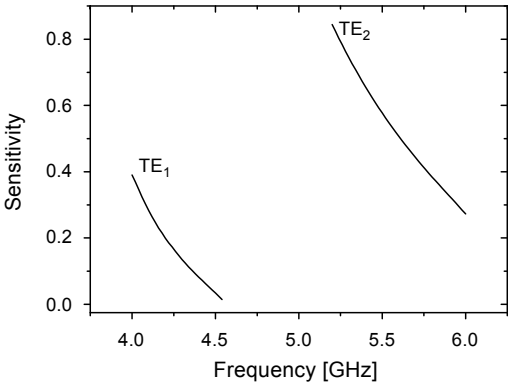

Fig. 6. Sensitivity *versus* angular frequency for the first and second guided modes when $h = 3.0$ cm. Other parameters are the same as in Fig. 2.

not sense any changes in the analyte index due to the propagation in the substrate layer. For thicknesses beyond the cut-off thickness, the sensitivity decreases as the figure shows and the modal index exceeds that of the substrate as the inset shows. In Fig. 6, the sensitivity was examined for a constant value of the film thickness ($h = 3.0$ cm) for the first and second guided modes. TE_1 mode was found in the operating frequency range 4.0 GHz $< \omega <$ 4.65 GHz whereas TE_2 mode was found in the frequency band 5.09 GHz $< \omega <$ 5.99 GHz. The sensitivity corresponding to the TE_1 ranged from 0.014 to 0.39 while it ranged from 0.27 to 0.84 for TE_2 mode. There is a considerable enhancement in the sensitivity of the second guided mode compared to that of the first one. It is worth mentioning that the two guided modes were not found for the same film thickness and guided light frequency.

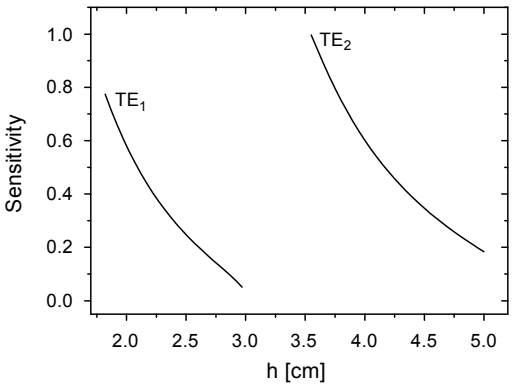

Fig. 7. Sensitivity *versus* guiding film thickness for the first and second guided modes for $\omega = 4.5$ GHz at which $n_{cz} = [(-3.93 + 0.13i)(-1.63 + 0.33i)]^{1/2}$. Other parameters are the same as in Fig. 2.

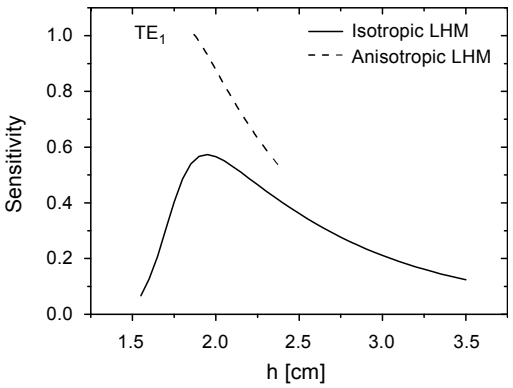

Fig. 8. Sensitivity *versus* guiding film thickness for isotropic and anisotropic DNM cladding for $\omega =$ $= 4.5$ GHz at which $n_{cz} = [(-3.93 + 0.13i)(-1.63 + 0.33i)]^{1/2}$. Other parameters are the same as in Fig. 2.

In a similar manner, Fig. 7 shows the sensitivity *versus* the film thickness for $\omega = 4.5$ GHz for TE_1 and TE_2 modes. The first mode was found to exist in the thickness h ranged between 1.82 to 2.97 cm and its corresponding sensitivity ranged between 0.05 to 0.77 whereas the second mode was found in the film thickness h ranged between 3.55 to 5.0 cm and it exhibited a sensing sensitivity in the range between 0.18 and 0.99.

It is worth investigating the effect of the anisotropy of the DNM cladding on the performance of the proposed sensor. Figure 8 shows the sensitivity *versus* the film thickness for TE_1 mode for anisotropic as well as isotropic DNM claddings. In the latter, the DNM was assumed to have $\varepsilon_{3x} = \varepsilon_{3y} = \varepsilon_{3z}$ which are given by Eq. (1) and $\mu_{3x} = \mu_{3y} = \mu_{3z}$ which are given by Eq. (2). When the DNM cladding is isotropic, the sensitivity showed a peak at an optimum value of h. It reached a maximum value

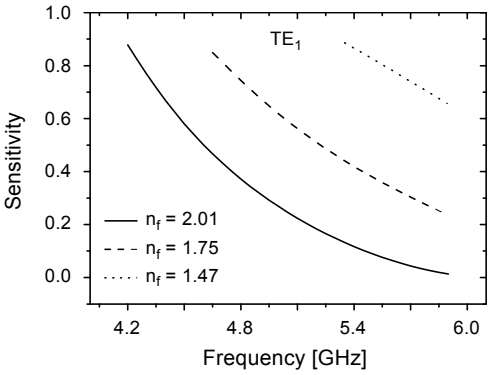

Fig. 9. Sensitivity *versus* angular frequency for the first guided mode for different guiding media. The waveguide parameters are the same as in Fig. 2.

of 57% at a thickness of 1.95 cm. On the other hand, when the DNM cladding is anisotropic, the sensitivity reached a maximum value of 100% at a thickness of 1.87 cm.

Finally, the sensitivity was investigated *versus* ω for three different guiding media: Si_3N_4 (n_f = 2.01), SiO_2-TiO_2 (n_f = 1.75), and Pyrex glass (n_f = 1.47) as shown in Fig. 9. For fixed ω, the sensitivity is considerably enhanced as the guiding film index decreases. For example for ω = 5.4 GHz, the sensitivities were 12%, 42%, and 87% for Si_3N_4, SiO_2-TiO_2, and Pyrex glass films, respectively. On the other hand, the operating frequency band is considerably reduced as the film index decreases. When the film was assumed Pyrex glass, the operating frequency band was 5.35 GHz < ω < 5.9 GHz which is a narrow band compared to 4.2 GHz < ω < 5.9 GHz for the Si_3N_4 film.

It is worth illustrating the coupler-sensitivity relationship. If we assume the input grating couplers, a guided mode can be excited if the wave vector components of the diffracted wave are equal to those of the guided mode. The incoupling efficiency ($\eta = P'/P$) is defined as the ratio of the power P' of the incoupled guided mode to the power P of the incident beam and it can be written as $\eta = \eta_m \hat{\eta}$, where η_m and $\hat{\eta}$ are the maximum incoupling efficiency and normalized incoupling efficiency, respectively. The incoupling efficiency is a function of the detuning variable denoted as $\overline{N}$ and this dependence has the form of a resonance curve of finite width $\delta\overline{N}$ [2]. For $\overline{N} = 0$, maximum incoupling efficiency occurs at which $\eta = \eta_m$ and $\hat{\eta}(\overline{N} = 0) = 1$. A change in $\overline{N}$ can be obtained by changing either the modal index of refraction of the guided mode or the angle of incidence. When the refractive index of an analyte changes, the modal index changes and the input grating coupler sensor responds to changes in the modal refractive index. This response can be observed in the change in the incoupling efficiency $\hat{\eta}(\overline{N})$. The sensitivity of the grating coupler sensor is determined by how much $\hat{\eta}(\overline{N})$ responds to the change in the refractive index of the analyte. In this case, the input grating coupler works as a refractometer. To determine the change in the analyte index, the shift of the angle of incidence of optimum incoupling is measured or the relative change $\Delta P'/P'$ of the incoupled power P' is determined using a detector.

4. Conclusion

In this work, a slab waveguide optical sensor utilizing anisotropic double negative material as a cladding layer was investigated. The measurand was assumed to be uniformly distributed in the substrate layer. The sensitivity of the sensor was studied with the frequency of the guided wave and thickness of the guiding film for different modes and waveguide configurations. The sensitivity was confirmed to be enhanced with decreasing the guided light frequency as well as the film thickness. At cut-off thickness, at which the modal index is equal to that of the substrate, the sensitivity reached 100%. For constant guiding film thickness, the sensitivity was dramatically enhanced with increasing the mode order of the guided wave. Moreover, for fixed frequency, the sensitivity of the second mode was found to be greater than that of the first one. The sensitivity was studied for three different guiding media and found to be improved as the guiding film index decreases, provided that the operating frequency band became narrower for low-index guiding media.

References

[1] Tiefenthaler K., Lukosz W., *Integrated optical switches and gas sensor*, Optics Letters **9**(4), 1984, pp. 137–139.

[2] Tiefenthaler K., Lukosz W., *Sensitivity of grating couplers as integrated-optical chemical sensors*, Journal of the Optical Society of America B **6**(2), 1989, pp. 209–220.

[3] Taya S.A., El-Agez T.M., *Comparing optical sensing using slab waveguides and total internal reflection ellipsometry*, Turkish Journal of Physics **35**(1), 2011, pp. 31–36.

[4] El-Agez T., Taya S., *Theoretical spectroscopic scan of the sensitivity of asymmetric slab waveguide sensors*, Optica Applicata **41**(1), 2011, pp. 89–95.

[5] Waechter H., Litman J., Cheung A.H., Barnes J.A., Loock H.-P., *Chemical sensing using fiber cavity ring-down spectroscopy*, Sensors **10**(3), 2010, pp. 1716–1742.

[6] Wenwei Niu, Ming Huang, Zhe Xiao, Jingjing Yang, *Nonlinear planar optical waveguide sensor loaded with metamaterials*, Optoelectronics and Advanced Materials: Rapid Communications **5**(10), 2011, pp. 1039–1045.

[7] Taya S.A., El-Farram E.J., El-Agez T.M., *Goos–Hänchen shift as a probe in evanescent slab waveguide sensors*, International Journal of Electronics and Communications (AEÜ) **66**(3), 2012, pp. 204–210.

[8] Kuswandi B., *Simple optical fibre biosensor based on immobilised enzyme for monitoring of trace heavy metal ions*, Analytical and Bioanalytical Chemistry **376**(7), 2003, pp. 1104–1110.

[9] Taya S.A., El-Agez T.M., *Slab waveguide sensor based on amplified phase change due to multiple total internal reflections*, Turkish Journal of Physics **36**(1), 2012, pp. 67–76.

[10] Udd E., *An overview of fiber-optic sensors*, Review of Scientific Instruments **66**(8), 1995, pp. 4015 –4030.

[11] Chien F.-C., Chen S.-J., *A sensitivity comparison of optical biosensors based on four different surface plasmon resonance modes*, Biosensors and Bioelectronics **20**(3), 2004, pp. 633–642.

[12] Homola J., Yee S.S., Gauglitz G., *Surface plasmon resonance sensors: Review*, Sensors and Actuators B: Chemical **54**(1–2), 1999, pp. 3–15.

[13] Kullab H.M., Taya S.A., *Transverse magnetic peak type metal-clad optical waveguide sensor*, Optik – International Journal for Light and Electron Optics **125**(1), 2014, pp. 97–100.

[14] Skivesen N., Horvath R., Pedersen H.C., *Optimization of metal-clad waveguide sensors*, Sensors and Actuators B: Chemical **106**(2), 2005, pp. 668–676.

[15] KULLAB H., TAYA S.A., EL-AGEZ T.M., *Metal-clad waveguide sensor using a left-handed material as a core layer*, Journal of the Optical Society of America B **29**(5), 2012, pp. 959–964.
[16] SKIVESEN N., HORVATH R., PEDERSEN H., *Peak-type and dip-type metal-clad waveguide sensing*, Optics Letters **30**(13), 2005, pp. 1659–1661.
[17] KULLAB H.M., TAYA S.A., *Peak type metal-clad waveguide sensor using negative index materials*, International Journal of Electronics and Communications (AEÜ) **67**(11), 2013, pp. 984–986.
[18] TAYA S.A., EL-AGEZ T.M., *Optical sensors based on Fabry–Perot resonator and fringes of equal thickness structure*, Optik – International Journal for Light and Electron Optics **123**(5), 2012, pp. 417–421.
[19] SKIVESEN N., HORVATH R., THINGGAAED S., LARSEN N.B., PEDERSEN H.C., *Deep-probe metal-clad waveguide biosensors*, Biosensors and Bioelectronics **22**(7), 2007, pp. 1282–1288.
[20] TAYA S.A., EL-AGEZ T.M., *A reverse symmetry optical waveguide sensor using a plasma substrate*, Journal of Optics **13**(7), 2011, article 075701.
[21] DENSMORE A., XU D.X., WALDRON P., JANZ S., CHEBEN P., LAPOINTE J., DELAGE A., LAMONTAGNE B., SCHMID J.H., POST E., *A silicon-on-insulator photonic wire based evanescent field sensor*, IEEE Photonics Technology Letters **18**(23), 2006, pp. 2520–2522.
[22] LU FA SHEN, JIA-CHENG QIU, ZI HUA WANG, *Guided modes in a slab waveguide with air core layer and left-handed materials claddings*, Progress in Electromagnetics Research Symposium Proceedings, Suzhou, China, September 12–16, 2011, pp. 1043–1048.
[23] VESELAGO V.G., *The electrodynamics of substances with simultaneously negative values of ε and μ*, Soviet Physics Uspekhi **10**(4), 1968, pp. 509–514.
[24] VALANJU P.M., WALSER R.M., VALANJU A.P., *Wave refraction in negative-index media: always positive and very inhomogenous*, Physical Review Letters **88**(18), 2002, article 187401.
[25] PENDRY J.B., HOLDEN A.J., ROBBINS D.J., STEWART W.J., *Magnetism from conductors and enhanced nonlinear phenomena*, IEEE Transactions on Microwave Theory and Techniques **47**(11), 1999, pp. 2075–2084.
[26] BOARDMAN A., EGAN P., VELASCO L., KING N., *Control of planar nonlinear guided waves and spatial solitons with a left-handed medium*, Journal of Optics A: Pure and Applied Optics **7**(2), 2005, pp. S57–S67.
[27] SHELBY R.A., SMITH D.R., SCHULTZ S., *Experimental verification of a negative index of refraction*, Science **292**(5514), 2001, pp. 77–79.
[28] PENG DONG, HONG WEI YANG, *Guided modes in slab waveguides with both double-negative and single-negative materials*, Optica Applicata **40**(4), 2010, pp. 873–882.
[29] TAYA S.A., EL-FARRAM E.J., ABADLA M.M., *Symmetric multilayer slab waveguide structure with a negative index material: TM case*, Optik – International Journal for Light and Electron Optics **123**(24), 2012, pp. 2264–2268.
[30] ZI HUA WANG, ZHONG YIN XIAO, SU PING LI, *Guided modes in slab waveguides with a left handed material cover or substrate*, Optics Communications **281**(4), 2008, pp. 607–613.
[31] TAYA S.A., QADOURA I.M., *Guided modes in slab waveguides with negative index cladding and substrate*, Optik – International Journal for Light and Electron Optics **124**(13), 2013, pp. 1431–1436.
[32] TAYA S.A., QADOURA I.M., EL-WASIFE K.Y., *Scaling rules for a slab waveguide structure comprising nonlinear and negative index materials*, International Journal of Microwave and Optical Technology (IJMOT) **7**(5), 2012, pp. 349–357.
[33] TAYA S.A., KULLAB H.M., QADOURA I.M., *Dispersion properties of slab waveguides with double negative material guiding layer and nonlinear substrate*, Journal of the Optical Society of America B **30**(7), 2013, pp. 2008–2013.
[34] BAE-IAN WU, GRZEGORCZYK T.M., YAN ZHANG, JIN AU KONG, *Guided modes with imaginary transverse wave number in a slab waveguide with negative permittivity and permeability*, Journal of Applied Physics **93**(11), 2003, p. 9386.

[35] ABADLA M.M., TAYA S.A., *Excitation of TE surface polaritons on metal–NIM interfaces*, Optik – International Journal for Light and Electron Optics **125**(3), 2014, pp. 1401–1405.
[36] ZHENG LIU, LIANGBIN HU, ZHIFANG LIN, *Enhancing photon tunnelling by a slab of uniaxially anisotropic left-handed material*, Physics Letters A **308**(4), 2003, pp. 294–301.
[37] TAO PAN, GUO-DING XU, TAO-CHENG ZANG, LEI GAO, *Study of a slab waveguide loaded with dispersive anisotropic metamaterials*, Applied Physics A **95**(2), 2009, pp. 367–372.
[38] CORY H., BARGER A., *Surface-wave propagation along a metamaterial slab*, Microwave and Optical Technology Letters **38**(5), 2003, pp. 392–395.
[39] LIANGBIN HU, CHUI S.T., *Characteristics of electromagnetic wave propagation in uniaxially anisotropic left-handed materials*, Physical Review B **66**(8), 2002, article 085108.
[40] TAYA S.A., ELWASIFE K.Y., *Guided modes in a metal-clad waveguide comprising a left-handed material as a guiding layer*, International Journal of Research and Reviews in Applied Sciences **13**(1), 2012, pp. 294–305.
[41] SHADRIVOV I.V., *Nonlinear guided waves and symmetry breaking in left-handed waveguides*, Photonics and Nanostructures – Fundamentals and Applications **2**(3), 2004, pp. 175–180.
[42] TAYA S.A., ELWASIFE K.Y., KULLAB H.M., *Dispersion properties of anisotropic-metamaterial slab waveguide structure*, Optica Applicata **43**(4), 2013, pp. 857–869.
[43] ZI HUA WANG, SU PING LI, *Quasi-optics of the surface guided modes in a left-handed material slab waveguide*, Journal of the Optical Society of America B **25**(6), 2008, pp. 903–908.
[44] KOSCHNY T., MOUSSA R., SOUKOULIS C.M., *Limits on the amplification of evanescent waves of left-handed materials*, Journal of the Optical Society of America B **23**(3), 2006, pp. 485–489.
[45] TAYA S.A., KULLAB H.M., *Optimization of transverse electric peak-type metal-clad waveguide sensor using double-negative materials*, Applied Physics A **116**(4), 2014, pp. 1841–1846.
[46] TAYA S.A., *Slab waveguide with air core layer and anisotropic left-handed material claddings as a sensor*, Opto-Electronics Review **22**(4), 2014, pp. 252–257.
[47] TAYA S.A., *P-polarized surface waves in a slab waveguide with left-handed material for sensing applications*, Journal of Magnetism and Magnetic Materials **377**, 2015, pp. 281–285.
[48] UPADHYAY A., PRAJAPATI Y.K., SINGH V., SAINI J.P., *Comprehensive study of reverse index waveguide based sensor with metamaterials as a guiding layer*, Optics Communications **348**, 2015, pp. 71–76.
[49] UPADHYAY A., PRAJAPATI Y.K., SINGH V., SAINI J.P., *Sensitivity estimation of metamaterial loaded planar waveguide*, Optical and Quantum Electronics **47**(7), 2015, pp. 2277–2287.

Received March 21, 2015
in revised form May 24, 2015